Excitation of multiphase waves of the nonlinear Schrödinger equation by capture into resonances

L. Friedland*
Racah Institute of Physics, Hebrew University of Jerusalem, Jerusalem 91904, Israel

A. G. Shagalov
Institute of Metal Physics, Ekaterinburg 620219, Russian Federation
(Received 13 September 2004; published 14 March 2005)

A method for adiabatic excitation and control of multiphase (N-band) waves of the periodic nonlinear Schrödinger (NLS) equation is developed. The approach is based on capturing the system into successive resonances with external, small amplitude plane waves having slowly varying frequencies. The excitation proceeds from zero and develops in stages, as an $(N+1)$-band ($N=0,1,2,\ldots$), growing amplitude wave is formed in the $(N+1)$th stage from an N-band solution excited in the preceding stage. The method is illustrated in simulations, where the excited multiphase waves are analyzed via the spectral approach of the inverse scattering transform method. The theory of excitation of 0- and 1-band NLS solutions by capture into resonances is developed on the basis of a weakly nonlinear version of Whitham's averaged variational principle. The phenomenon of thresholds on the driving amplitudes for capture into successive resonances and the stability of driven, phase-locked solutions in these cases are discussed.

DOI: 10.1103/PhysRevE.71.036206 PACS number(s): 89.75.Kd, 05.45.Xt, 05.45.Yv, 52.35.Mw

I. INTRODUCTION

The nonlinear Schrödinger (NLS) equation

$$i\psi_t + \psi_{xx} + 2\sigma|\psi|^2\psi = 0, \quad \sigma = \pm 1 \tag{1}$$

is one of the most important equations of nonlinear physics. It describes a large number of physical phenomena in nonlinear optics, plasma physics, and water waves (for an introduction to some of the problems see [1]). The discovery of the inverse scattering transform (IST) method [2] and its version for the NLS problem [3] allowed better understanding of the multiplicity of solutions of this important equation. However, only the most simple NLS solutions, such as plane waves, cnoidal waves, and solitons, have attracted great attention of the physics community. More complex NLS constructs, particularly *multiphase* waves (referred to as "N-band" solutions [4] within the IST approach), remained inaccessible in applications. The reason was the difficulty of realization of very special initial conditions for formation of these solutions [5]. In the present work, a simple and, we believe, realizable procedure of generating multiphase waves of spatially periodic NLS equation is suggested. The approach can be referred to as pattern formation by synchronization (or PFS). The idea is to replace Eq. (1) by the perturbed problem

$$i\psi_t + \psi_{xx} + 2\sigma|\psi|^2\psi = \varepsilon f(x,t), \quad \varepsilon \ll 1 \tag{2}$$

and, by starting from some simple (even trivial, $\psi \equiv 0$) initial conditions, to find drive function $\varepsilon f(x,t)$ such that one reaches a vicinity of the desired nontrivial (N-band) solution of the unperturbed system in the process of evolution. Counterintuitively, our goal is to excite a *large* amplitude, nontrivial NLS wave, say from zero, by applying a *small* perturbation. The smallness of the drive term, however, does not prevent finding a solution to this problem, if the desired excitation process occurs during a sufficiently long period of time. In fact, we shall see below that successive use of simple perturbing terms in the form of plane waves with slowly varying (chirped) frequencies allows stable generation of N-band waves of spatially periodic NLS equation with a desired number of phases. We believe that this approach opens a new window for applications in many systems described by the NLS equation.

The physical mechanism in our approach involves capture into resonances and adiabatic synchronization (phase-locking) in the driven system. First applications of the method to extended systems included formation of weakly nonlinear plasma waves [6] and solitons of the Korteweg–de Vries (KdV) equation [7] by starting *in* resonance, as well as, 2- and 3-wave interactions in nonuniform media [8,9] both phenomena involving *passage through* resonance. Later, adiabatic synchronization was used in sine-Gordon systems [10,11], for generation of cnoidal and standing NLS waves [12,13] and in fluid dynamics [14–16]. Most recently, a similar approach allowed formation of multiphase solutions of the Korteweg–de Vries (KdV) equation [17] and Toda chain [18]. Here, for the first time, we apply the PFS idea to multiphase NLS waves. We shall see how the NLS system driven by small amplitude, chirped frequency plane waves is captured into resonances, leading, at certain conditions, to a persisting phase-locking (the term wave *autoresonance* can be used in this situation) despite the variation of the driving frequencies. As the result of this synchronization, the solution evolves in the solution space of the unperturbed NLS equation, and new phases are added to the driven wave in successive excitation stages. At the end of the process, the solution arrives at the vicinity of a multiphase NLS wave, having a prescribed set of wave numbers and frequencies.

The scope of the paper will be as follows. Section II will illustrate our approach in numerical simulations. We shall

*Electronic address: lazar@vms.huji.ac.il

use the spectral theory of the IST [19] in this section for interpreting the numerical results. Our theoretical analysis proceeds in Sec. III, by considering excitation of simplest, plane wave (0-band) solutions by synchronization. In the same section we shall discuss a universal problem of thresholds for synchronization, characterizing the PFS paradigm in this and many other applications. Section IV will be devoted to the theory of autoresonant excitation of 1-band solutions by successive passage through two resonances. The excitation of 1-band waves will proceed from generation of a large amplitude plane wave by starting from zero as in Sec. III, followed by autoresonant formation of a 1-band NLS solution by passage through another resonance. The theory of this process will be based on a weakly nonlinear version of Whitham's averaged variational principle [20] for autoresonant waves (Secs. IV A and IV B). We shall also study the problem of thresholds on the driving amplitude for synchronization in this problem (Sec. IV C), as well as the stability of the driven wave (Sec. IV D). Finally, Sec. V will present our conclusions.

II. SYNCHRONIZATION BY PASSAGE THROUGH RESONANCES: NUMERICAL SIMULATIONS

We proceed by presenting the results of numerical solutions of Eq. (2) with a properly chosen right-hand side (RHS) for excitation of N-band waves. The goal is to use simple initial conditions and generate approximately the following unperturbed NLS solution (see Appendix A)

$$\psi = U(\Theta_1, \Theta_2, \dots)\exp\{i[\xi + V(\Theta_1, \Theta_2, \dots)]\}, \qquad (3)$$

where U and V are 2π-periodic real functions of N-phases $\Theta_i = K_i x - \Omega_i t$, $i = 1, \dots, N$, wave numbers K_i and frequencies Ω_i are constant, while $\xi = K_0 x - \Omega_0 t$ (the *external* phase) appears in the complex exponential in Eq. (3) only. We shall assume L-periodicity in x in the problem, so both ψ and f in Eq. (2) are L-periodic in x, and all $K_i = n_i k_0$, where n_i are integers, $k_0 = 2\pi/L$ being the principal wave number.

Our numerical procedure for generating N-band solutions is as follows. We start with zero initial conditions and solve the perturbed NLS equation (2), where the driving function is a plane wave $f_0 = \exp\{i[m_0 k_0 - \int \omega_0(t)dt]\}$ (we use $m_0 = 0$ below, as an example) having slowly varying frequency $\omega_0(t) = \omega_{0r} - \alpha_0 t$, where α_0 is a constant chirp rate, and $\omega_{0r} = (m_0 k_0)^2$ is the linear resonance frequency of the unperturbed NLS equation. Importantly $\mathrm{sgn}(\alpha_0) = \sigma$. This slow passage through resonance at $t = 0$ will excite a slightly perturbed plane wave (0-band solution) [12] with amplitude and phase [external phase in Eq. (3)] controlled by the chirped driving frequency. We shall discuss this stage of excitation in Sec. III in more detail.

When the amplitude of the 0-band solution reaches, at $t = t_1$, some value $U(t_1) = A_0$, we switch off drive f_0 and apply a new drive, $f_1 = \exp\{i[m_1 k_0 x - \int \omega_1(t)dt]\}$ ($m_1 = 1$ in our examples below), where the slow frequency $\omega_1(t) = \omega_{1r} - \alpha_1 t$ passes (at $t = 0$) through another resonance, $\omega_{1r} = -2\sigma A_0^2 + m_1 k_0 \sqrt{(m_1 k_0)^2 - 4\sigma A_0^2}$ (see Sec. IV for details) with the excited 0-band solution. When chirp rate α_1 is sufficiently small, this passage through resonance will create a growing amplitude 1-band solution (see our example below and the discussion in Sec. IV) which is continuously phase-locked to f_1.

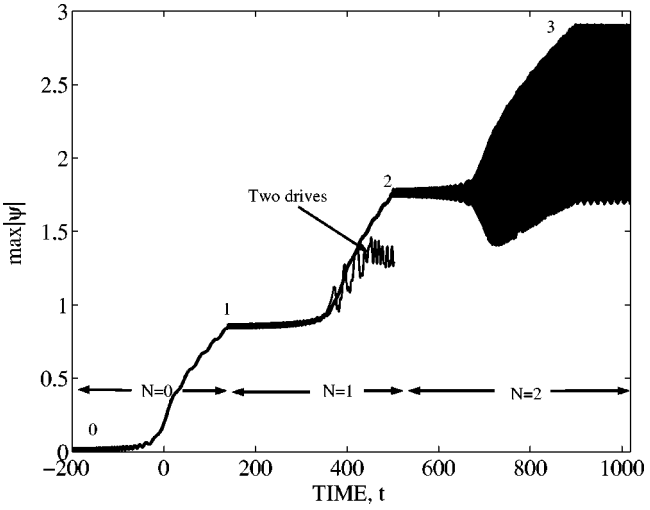

FIG. 1. The evolution of the maximum $|\psi|$ over the periodicity length in the three-stage excitation process of a multiphase NLS wave (thick line). The time intervals of emergence of $N = 0, 1, 2$-band solutions are shown by arrows. The numbers along the line indicate the times of switching different drive terms on and off. The thin line represents saturated excitation case when two drives are present at a time in the second excitation stage.

Next, at some excitation stage we switch off drive f_1 and replace it by a new chirped frequency drive $f_2 = \exp\{i[m_2 k_0 x - \int \omega_2(t)dt]\}$ ($m_2 = 2$ in our examples below) creating a growing amplitude 2-band solution, as the new driving frequency passes the next resonant value ω_{2r}, and so on. By repeatedly applying this switching on and off driving procedure with drives of form of a plane wave (only one drive is present at a time),

$$\varepsilon f_j = \varepsilon \exp\left\{ i\left[m_j k_0 x - \int \omega_j(t)dt \right] \right\} = \varepsilon \exp(i\varphi_{dj}), \qquad (4)$$

where m_j is an integer, while the driving frequency $\omega_j(t)$ passes through the resonance with the wave excited in the preceding stage, one can generate an N-band solution with a desired number of internal phases. We illustrate this procedure in Figs. 1 and 2 showing a three stage excitation process, leading to a 2-band, focusing ($\sigma = +1$) NLS solution. Our simulations used a standard pseudospectral method [21]. The number of harmonics varied up to 256. The accuracy was tested by increasing the number of discretization points in both time and space.

Figure 1 presents the evolution of the maximum over periodicity length L ($L = \pi$ in the simulations) value of $|\psi| = U$ [see Eq. (3)], while Fig. 2 shows the color contour map of $|\psi|$ in three small time windows, $\Delta t = 5.2$, at the ends of different stages of evolution, denoted by numbers 1,2,3 along the graph in Fig. 1. We used $\varepsilon = 0.02$, all chirp rates $\alpha_i = 0.01$, and three successive drives of form (4) with $m_j = 0$, 1, and 2. Only one drive was present in each excitation stage (time

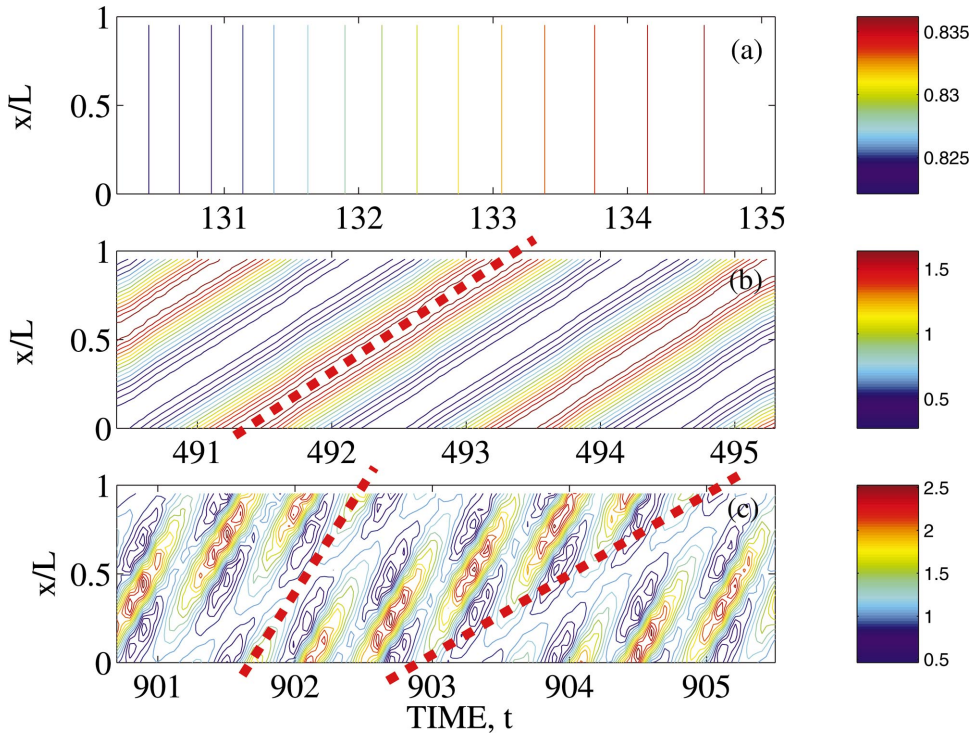

FIG. 2. (Color) The spatio-temporal structure of the solution for $|\psi|$ in three small time windows around times indicated by numbers 1, 2, and 3 in Fig. 1 at different stages of excitation. (a) $|\psi|=$const equidistant contour lines at the end of the first excitation stage (the plane wave solution). The color of each line corresponds to the value of $|\psi|$ on this line as shown in the corresponding color bar at the right. The vertical lines illustrate spatially uniform, slowly time varying amplitude of the solution ($0.82<|\psi|<0.84$ in the chosen time window, as seen in the corresponding color bar). (b) $|\psi|=$const contour lines at the end of the second excitation stage (1-band solution). $|\psi|$ remains constant along the direction indicated by the red dashed line in the figure. The internal phase of the solution remains constant along this line. (c) $|\psi|=$const contour lines at the end of the third excitation stage (2-band solution). $|\psi|$ is singly-periodic in time along two characteristic directions of constancy (red dashed lines in the figure) of one of the two internal phases of the solution.

intervals $[-200,140]$, [140, 500], and [500, 900]) and the corresponding driving frequency passed a resonance with the wave created in the preceding time interval, leading to the addition of a new phase in the solution (see below). We observe that the maximum $|\psi|$ increases (in average) in every new stage of excitation. Also, $|\psi|$ is nearly a constant (0.83) in Fig. 2(a), i.e., the driven solution comprises a slightly perturbed plane wave at the end of the first stage of excitation. In contrast, Fig. 2(b) (the end of the second excitation stage) illustrates the emerging 1-phase solution, such that $|\psi|=U(\Theta_1)$ remains constant along the direction shown by the red dashed line in Fig. 2(b), i.e., along the characteristics $dx/dt=\Omega_1/K_1$ associated with its phase $\Theta_1=K_1x-\Omega_1t$. Finally, at the end of the third stage [Fig. 2(c)] one observes a more complicated pattern, which is nearly periodic along *two* main directions (shown by red dashed lines). This indicates a 2-phase solution, $U=U(\Theta_1,\Theta_2)$, which becomes a singly-periodic function of time along characteristic directions $dx/dt=\Omega_1/K_1$, or Ω_2/K_2, along which one of the two phases remains constant. Finally, the thin line in Fig. 1 shows the numerical result for the same set of parameters and initial conditions as above, but with drive f_0 (at a constant frequency) present in addition to f_1 in the second excitation stage. We see that the amplitude saturates in this case and the continuing variation of the driving frequency does not lead to a growing amplitude solution. We have found a similar effect at all stages of excitation, when two drives have been present at a time. The observed saturation is due to instability of the driven solution and we shall discuss this instability for $N=0,1$ cases (as in Fig. 1) in more detail in Sec. IV.

For further clarification of our multistage excitation process, we have analyzed the numerical solutions by means of the spectral approach of the IST. Only a necessary minimum of information about this method is presented below for completeness. It is known [19] that N-band NLS solutions can be constructed via a set of $2(N+1)$ parameters λ_k (the main spectrum) and a set of N variables $\mu_j(x,t)$ (auxiliary spectrum). The main spectrum of the unperturbed NLS is constant in time and, for the focusing NLS ($\sigma=+1$), consists of $N+1$ different complex-conjugate pairs in the complex plane, while in the defocusing case ($\sigma=-1$), λ_k are $2N+2$ real numbers. The auxiliary spectrum components are functions depending on space and time via N phases Θ_n of the N-band solution. In other words, $\mu_j=\mu_j(\Theta_1,\Theta_2,\ldots,\Theta_N)$. If all λ_k and μ_j and the value of ψ are given at initial time t_0 and position x_0, then the corresponding N-band solution can be constructed by solving a set of first order ordinary differential equations in x and t [19] (see Appendix A). On the other hand, given an N-band solution ψ at some time t, one can calculate the corresponding IST spectra by solving certain linear eigenvalue problems. The main spectrum of a general solution of the periodic NLS is characterized by an in-

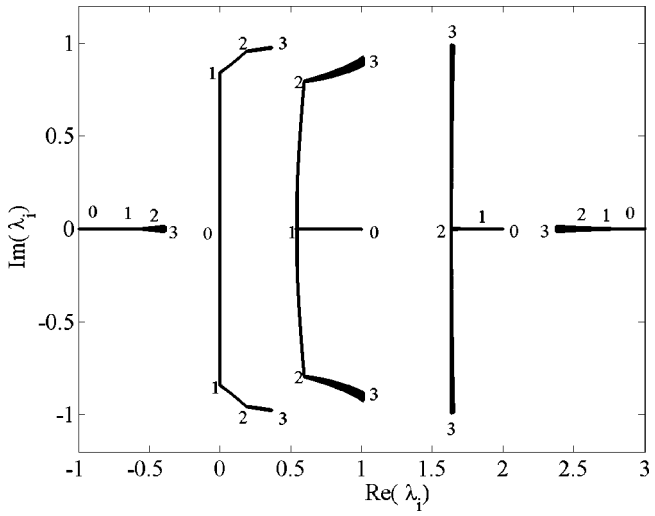

FIG. 3. The evolution of five pairs of the main spectrum of the driven solution shown in Figs. 1 and 2 in the complex plain. The segments 0-1, 1-2, 2-3, and 3-4 display evolution in subsequent time intervals of excitation of 0, 1, and 2-band solutions during the three excitation stages indicated by the same numbers in Fig. 1. One can see the removal of degeneracy of an additional pair in the main spectrum in each excitation stage, corresponding to appearance of a new phase in the solution. All other pairs of the main spectrum remain degenerate.

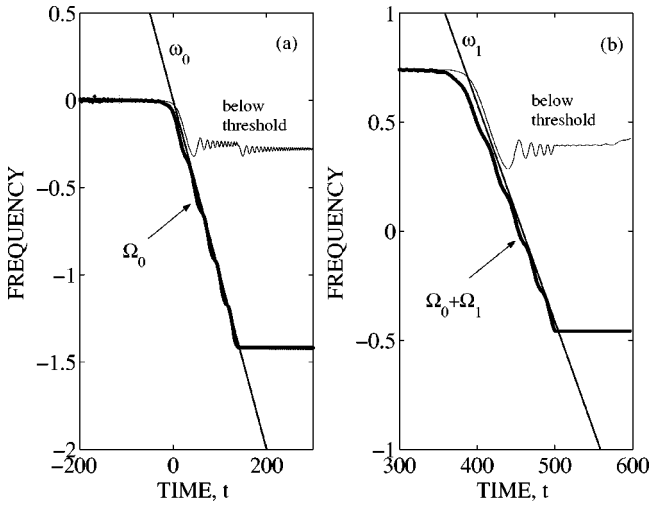

FIG. 4. The frequencies locking in the first two stages of excitation in Fig. 1. The frequencies $\Omega_{0,1}$ of the driven wave are found via the main IST spectrum of the driven solution. (a) $\Omega_0 \approx \omega_0$ (thick line) in the first excitation stage beyond the linear resonance ($t>0$). (b) $\Omega_0+\Omega_1 \approx \omega_1$ in autoresonance thick line (blue) in the second excitation stage. The tilted straight lines show chirped driving frequencies. The thin lines in (a) and (b) illustrate dephasing of the excited wave for the driving amplitudes below the thresholds for synchronization.

finite number of pairs of constant eigenvalues λ, however, for the N-band solution, only $N+1$ such pairs are *nondegenerate* and needed for construction of the solution as described above. Thus, counting the number of nondegenerate pairs of the main spectrum, allows to diagnose the number of phases in the corresponding solution. We use this idea in our application as follows. We solve the driven NLS equation numerically and view our numerical solution (at a given time) as the initial data for some solution of the unperturbed NLS. From this data we calculate the main spectrum via a discrete approximation of the scattering problem [22]. We expect to see $N+1$ nondegenerate pairs in the main spectrum and many nearly degenerate pairs, if our driven solution is near some large amplitude N-band solution of the unperturbed NLS. Figure 3 shows the evolution path (in the complex plane) of the main spectrum corresponding to the solution of the driven problem shown in Figs. 1 and 2. The numbers 0, 1, 2, and 3 in the figure show the location of the main spectrum values at different times of evolution represented by the same numbers in Fig. 1. One can see that a new pair of values in the spectrum becomes nondegenerate at each stage of excitation and the final solution (at time indicated by number 3 in Figs. 1 and 3) is a slightly perturbed 2-band solution (its main spectrum has *three* nondegenerate pairs of complex values).

Next, we illustrate that our driven solution satisfies particular phase-locking relations with the driving waves at different excitation stages. For example, in the first stage (0-band, plane wave solution), the phase locking is between the driving and the external phases, i.e., $\xi \approx \varphi_{d0}$. In contrast, in the second stage (excitation of the 1-band solution) the phase-locking involves a triad of phases, i.e., $\xi+\Theta_1 \approx \varphi_{d1}$. We illustrate these two phase-locking relations in Figs. 4(a) and 4(b). The spectral theory connects between the frequencies and wave numbers of the N-band solutions and the IST spectra [4]. In cases $N=0$ and 1, these connections are simple (see Appendix A). For example, if $\lambda_1^{\pm}=a_1 \pm ib_1$ is the relevant *nondegenerate* pair of the main spectrum of the plane wave ($N=0$), then

$$K_0 = -2a_1, \quad \Omega_0 = 4a_1^2 - 2b_1^2. \tag{5}$$

The driving wave has zero wave number in the first excitation stage in our example in Figs. 1–3. Therefore, $K_0=0$ in the excited solution, and, from Eq. (5), $a_1=0$ (this result can be seen in the spectrum in Fig. 3 between points 0 and 1). Therefore, the above-mentioned phase locking, $\xi \approx \varphi_{d1}$, is equivalent to condition $\Omega_0(t)=-2b_1^2 \approx \omega_0(t)$. Fig. 4(a) shows the numerically found evolution of $-2b_1^2$ (full thick line) and compares it with the chirped driving frequency (dotted line). One observes the continuing phase locking (autoresonance) in the system beyond the linear resonance ($t>0$). The phase locking is destroyed and Ω_0 stays constant after the first stage drive is switched off at $t=140$. One can also see slow oscillating modulations of $\Omega_0(t)$ in autoresonance around the linearly decreasing averaged value (the latter follows the variation of the driving frequency). These modulations comprise another characteristic feature of autoresonance in the system (see Sec. III). Next, for $N=1$, with two nondegenerate pairs of the main spectrum, $\lambda_{1,2}^{\pm}=a_{1,2} \pm ib_{1,2}$, we have (see Appendix A)

$$K_0 = 2\langle \mathrm{Re}(\mu_1)\rangle - s, \quad \Omega_0 = q - 2s\langle \mathrm{Re}(\mu_1)\rangle, \tag{6}$$

and $\Omega_1=sK_1$, where $s=2(a_1+a_2)$, $q=4(a_1^2+a_2^2+a_1a_2)-2(b_1^2+b_2^2)$, and $\langle \cdots \rangle$ denotes averaging over one oscillation of the

internal phase. Since, again, $K_0=0$ and $K_1=k_0$ (the same as the wave number in the second stage drive), we have $2\langle \mathrm{Re}(\mu_1)\rangle = s$. Therefore,

$$\Omega_0 = -2(b_1^2 + b_2^2 + 2a_1a_2), \quad \Omega_1 = 2(a_1 + a_2)k_0. \tag{7}$$

We test the phase-locking in the second excitation stage in Fig. 4(b), by comparing $\Omega_0+\Omega_1$ found from the main spectrum via Eqs. (7) with the driving frequency $\omega_1(t)$. Again, we observe efficient phase-locking and the characteristic autoresonant oscillations around linearly varying average value of $\Omega_0+\Omega_1$ in Fig. 4(b) for times $t>390$, i.e., beyond the linear resonance ($\omega_1=\omega_{r1}$; see Sec. IV). This phase-locking discontinues at $t=500$, as the second driving wave is switched off. We shall present the theory of the phase-lockings in $N=0$ and 1 stages in Secs. III and IV.

The frequency-locking diagrams of the type shown in Fig. 4 allow us to demonstrate another important phenomenon associated with our excitation scheme, i.e., the existence of thresholds on the driving amplitudes for capturing the system into resonance. We have repeated the calculations for the same parameters as above, but $\varepsilon_0=0.009$ [in Fig. 4(a)] and $\varepsilon_1=0.007$ [in Fig. 4(b)], which are just below the corresponding threshold amplitudes [$\varepsilon_{0,1}^{th}=0.0092, 0.0072$, see Eqs. (12) and (50) below] and show the results by thin lines. One can see that the phase locking in both cases discontinues, shortly beyond the linear resonances. We shall find expressions for these thresholds in Secs. III and IV.

Our final illustration of PFS in the NLS system shows the case of the defocusing NLS equation ($\sigma=-1$). We performed simulations with the same parameters for the defocusing case as in Figs. 1–4 but reversed the signs of the driving frequency chirp rates and added an additional (fourth) excitation stage with $k_4=-k_0$, $\varepsilon_3=0.02$, and $\alpha_3=-0.01$ in time interval [900,1200]. Figure 5(a) shows the evolution of the maximum $|\psi|$ until the arrival at the final 3-band solution. The successive emergence of four nondegenerate pairs of main spectrum components in the defocusing NLS system is illustrated in Fig. 5(b). The main spectrum is real in this case and Fig. 5(b) shows the actual time evolution of the spectrum, where each new phase in the solution corresponds to the removal of one degeneracy.

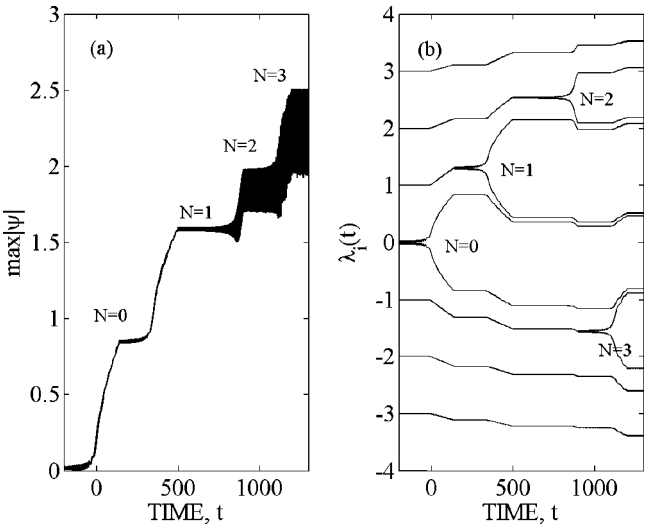

FIG. 5. Excitation of the multiphase solution via synchronization in the case of defocusing NLS equation. The parameters and initial conditions are the same as in Fig. 1, but the signs of the driving frequency chirp rates are opposite and an additional (fourth) excitation stage (3-band solution) with $k_4=-k_0$, $\varepsilon_3=0.02$, and $\alpha_3=-0.01$ in time interval [900,1200] is added in the simulation. (a) Maximum $|\psi|$ over periodicity length versus time; (b) the successive opening of 4 gaps in the main spectrum (all real) as one passes different resonances in the process of evolution.

III. EXCITATION OF PLANE NLS WAVES AND THRESHOLD PHENOMENON

The starting point of our theory is the problem of excitation and control of plane NLS waves by synchronization. This problem was first discussed in Ref. [12], but the issue of thresholds for synchronization by passage through resonance was raised for the first time later in seemingly unrelated, nonneutral plasma experiments [23]. Here, we focus on the thresholds for capture of plane NLS waves into resonance.

Consider the driven NLS system,

$$i\psi_t + \psi_{xx} + 2\sigma|\psi|^2\psi = \varepsilon \exp\{i[\kappa x - \phi_0(t)]\}, \tag{8}$$

where $\kappa=mk_0$ and the driving frequency $\omega_0=d\phi_0/dt=\omega_{0r}-\alpha t$ is chirped linearly in time. We seek a time modulated plane wave solution of Eq. (8) of form $\psi=U(t)\exp(i\xi)$, where amplitude $U>0$, and phase $\xi=\kappa x-\chi(t)$ is real. Then,

$$iU_t + (\chi_t - \kappa^2 + 2\sigma U^2)U = \varepsilon \exp\{i(\chi - \phi_0)\}$$

or, by separating the real and imaginary parts and defining phase mismatch $\Phi=\phi_0-\chi$,

$$U_t = -\varepsilon \sin\Phi, \tag{9}$$

$$\Phi_t = \omega_{0r} - \kappa^2 - \alpha t + 2\sigma U^2 - \frac{\varepsilon}{U}\cos\Phi. \tag{10}$$

Finally, we choose $\omega_{0r}=\kappa^2$ (the driving perturbation passes linear resonance at $t=0$), correlate the sign of the chirp rate $\alpha=\sigma|\alpha|$ with σ, and introduce new time variable $\tau=|\alpha|^{1/2}t$, and amplitude, $A=2^{1/2}|\alpha|^{-1/4}U$. Then Eqs. (9) and (10) can be combined into the following equation for $\Psi=A\exp(i\Phi)$:

$$i\Psi_\tau + \sigma(|\Psi|^2 - \tau)\Psi = \eta, \tag{11}$$

where $\eta=2^{1/2}|\alpha|^{-3/4}\varepsilon$. Remarkably, this *single* parameter (η) system, describing capture into resonance and synchronization in the present application, also characterizes synchronization of 1-band NLS waves into resonance (see Sec. IV), and related PFS problems in plasmas [23], fluid dynamics [14], planetary dynamics [24], and atomic physics [25,26]. Thus, Eq. (11) is a fundamental equation of the PFS paradigm. In studying passage through the linear resonance at $\tau=0$, we seek asymptotic solutions of this equation at large positive τ subject to zero initial condition at large negative τ. The analysis shows (see discussion of a similar problem in [14]) that two such asymptotic solutions may emerge after passage through resonance, i.e., either (a) constant amplitude (bounded) solution $\Psi=A_0\exp(-i\sigma\tau^2/2)$, or (b) the un-

bounded solution, $\Psi = \pm\tau^{1/2}$. The phase mismatch $\Phi = \sigma\tau^2$ between the driven and driving waves for the bounded solution grows quadratically in time. It is this increasing mismatch, which leads to the amplitude saturation at A_0 after passage through resonance. In contrast, for the unbounded solution, the mismatch remains constant (either $\Phi = 0$ or π), meaning a perfect phase locking in the driven system, as the amplitude grows continuously beyond the linear resonance. In other words, the driving frequency shift τ is balanced by the nonlinear frequency shift $|\Psi|^2$ in Eq. (11) continuously, so that the system stays in resonance despite the variation of the driving frequency. This is the desired autoresonant solution in the problem. But how the system chooses between the bounded and phase-locked, growing amplitude states and what determines the phase mismatch value $\Phi = 0$ or π in the latter case? One finds that the transition of the system to autoresonance is controlled by single parameter η in Eq. (11), while Φ asymptotically approaches 0 or π depending on the sign of σ. Numerically, the transition occurs for $\eta > \eta_{th} = 0.411$ [26] (a more physical line of arguments [14] using a dynamical picture of resonant interaction yields a slightly higher approximate threshold value $\eta_{th} \approx 3^{-3/4} = 0.438$). By returning to our original parameters, we obtain the threshold driving amplitude

$$\varepsilon_{th} = 0.291|\alpha|^{3/4}. \tag{12}$$

For $\varepsilon > \varepsilon_{th}$ the system is always in autoresonance, i.e., its amplitude U grows as $t^{1/2}$ at large positive t, while phase mismatch $\Phi \approx 0$ (for $\sigma = +1$) and π (for $\sigma = -1$) in average. The theory [14] also shows that at finite times, in addition to the smooth averaged evolution described above, both the amplitude and the phase mismatch perform slow oscillations around the average with characteristic frequency ν scaling as

$$\nu \approx 2\sqrt{\varepsilon U} = \sqrt{2\eta|\alpha|A}. \tag{13}$$

One can see the predicted $t^{1/2}$ growth of the amplitude, as well as the slow autoresonant oscillations in our simulation results in Figs. 1 and 4 in the first (0-band) stage of excitation. This completes our discussion of passage through resonance and synchronization of plane NLS waves and we proceed to synchronized 1-band solutions.

IV. AUTORESONANT EXCITATION AND STABILITY OF 1-BAND WAVES

A. Reduced, weakly nonlinear problem

Consider the driven problem in the second stage of excitation in Fig. 1,

$$i\psi_t + \psi_{xx} + 2\sigma|\psi|^2\psi = \varepsilon \exp(i\varphi_{d1}), \tag{14}$$

where $\varphi_{d1} = mk_0x - \phi_1(t)$, and $d\phi_1/dt = \omega_1(t) = \omega_{1r} - \alpha t$. This equation is similar to Eq. (8), but, instead of zero initial conditions, we proceed from the plane wave solution excited in the first stage, as described in Sec. III. We shall limit discussion to $m = 1$ case for simplicity. We write the driven solution as $\psi = U\exp(i\theta)$, $U > 0$, Im $\theta = 0$, and separate the real and imaginary parts in Eq. (14):

$$U_t + \theta_{xx}U + 2\theta_xU_x + \varepsilon \sin(\varphi_{d1} - \theta) = 0, \tag{15}$$

$$\theta_tU - U_{xx} + \theta_x^2U - 2\sigma U^3 + \varepsilon \cos(\varphi_{d1} - \theta) = 0. \tag{16}$$

This system can be also obtained from the variational principle

$$\delta\left(\int\int dxdtL(U, U_x, U_t, \theta_x, \theta_t, t)\right) = 0, \tag{17}$$

where Lagrangian $L = L_0 + L_1$,

$$L_0 = \frac{1}{2}[U_x^2 + U^2(\theta_x^2 + \theta_t)] - \frac{1}{2}\sigma U^4, \tag{18}$$

and $L_1 = \varepsilon U\cos(k_0x - \phi_1 - \theta)$. Since the unperturbed Lagrangian L_0 depends on θ_x, θ_t but not on θ (θ is the potential) one can conveniently approach our problem by using Whitham's averaged variational principle [20]. Generalization of this approach to autoresonantly driven two-component fields was developed in [27] and applied to some NLS cases in [12]. The method describes slow space-time modulations of driven, rapidly oscillating fields and uses the small slowness parameter associated with these modulations in developing a perturbation theory, yielding evolution equations of relevant slow field variables. In the NLS application [12], one writes the solution as

$$\psi = U(\Theta, t)\exp\{i[\xi + V(\Theta, t)]\}, \tag{19}$$

where $\xi = K_0x - \int\Omega_0(t)dt$, both U and V are 2π-periodic in the fast phase variable $\Theta = K_1x - \int\Omega_1(t)dt$, $K_1 = mk_0$, while the explicit time dependence in U and V, as well as in frequencies $\Omega_{0,1}(t)$ is assumed to be slow. Note that Eq. (19) has the form of a slowly modulated 1-band solution [see Eq. (A6) in Appendix A]. By Whitham's approach, instead of working with the exact Lagrangian, one averages L over Θ between 0 and 2π, defining the averaged Lagrangian $\Lambda = \langle L\rangle_\Theta$. Then $\Lambda = \Lambda(P, \xi_x, \xi_t, \Theta_x, \Theta_t, \Phi)$ becomes a function of a set P of slow dependent variables (see Appendix B), as well as of phases ξ and Θ, entering Λ either via the slow frequencies $\Omega_{0,1}$ and wave vectors or the slow phase mismatch Φ [12] (we shall see below that $\Phi = \Theta + \xi - \varphi_{d1}$ in the case of interest). Lagrangian Λ is used in the averaged variational principle

$$\delta\left(\int\int dxdt\Lambda(P, \xi_x, \xi_t, \Theta_x, \Theta_t, \Phi)\right) = 0, \tag{20}$$

where now x and t are *slow* space-time variables. Then, to the desired order of our perturbation scheme, variations with respect to all independent variables, P, ξ, Θ, yield a set of slow evolution equations describing capture into resonance and synchronization in the problem.

Here, focusing primarily on the initial autoresonance stage describing the threshold for synchronization in generating 1-band solutions, we shall adopt a simplified, weakly nonlinear version of the averaged variational principle. The idea is to expand U and V in Eq. (19) in Fourier series in Θ, keep the lowest significant number of terms (zero and first two harmonics) in the series, substitute the result in L, and calculate weakly nonlinear Λ by averaging over Θ. The proper expansion is (see Appendix B)

$$U \approx u_0 + u_1 \cos\Theta + u_2 \cos 2\Theta, \tag{21}$$

$$V \approx -v_1 \sin\Theta - v_2 \sin 2\Theta, \tag{22}$$

where we assume the following ordering of the slow amplitudes u_i and v_i: u_0 may be of $O(1)$, $|u_1|$, $|v_1| \ll 1$, and u_2, $v_2 \sim O(u_1^2)$. With these definitions, the averaged Lagrangian Λ depends on seven independent variables $P=\{u_{0,1,2}, v_{1,2}\}$, Θ, and ξ [we shall assume $\xi=-\int\Omega_0(t)dt$ in this application] and becomes, to $O(u_1^4)$ [see Eqs. (B7)–(B12) in Appendix B],

$$\Lambda = -\frac{\sigma}{2}\Lambda_0 - \frac{\Omega_0}{4}\Lambda_1 + \frac{\Omega_1}{4}\Lambda_2 + \frac{K_1^2}{4}\Lambda_3 + \Lambda_d, \tag{23}$$

where

$$\Lambda_0 = u_0^4 + 3u_0u_1^2u_2 + 3u_0^2(u_1^2+u_2^2) + 3u_1^4/8, \tag{24}$$

$$\Lambda_1 = 2u_0^2 + u_1^2 + u_2^2, \tag{25}$$

$$\Lambda_2 = 2u_0u_1v_1 + u_1v_1u_2 + u_1^2v_2 + 4u_0u_2v_2, \tag{26}$$

$$\Lambda_3 = u_1^2 + 4u_2^2 + v_1^2(u_0^2 + 3u_1^2/4 + u_0u_2) + 4u_0u_1v_1v_2 + 4u_0^2v_2^2, \tag{27}$$

and the driving term

$$\Lambda_d = \frac{\varepsilon}{2} s \cos\Phi, \tag{28}$$

where $s=(u_1-u_0v_1)$ and $\Phi=\Theta+\xi-\varphi_{d1}$.

B. Variational equations

At this stage we write the variational equations in the problem. We start from variation in Eq. (20) with respect to u_0. This yields [to $O(u_1^2)$] expression

$$2u_0^2 = -\sigma\Omega_0 - 3u_1^2 \tag{29}$$

and, to zero order, $u_{00}^2=-(\sigma/2)\Omega_{00}$. Similarly, variations with respect to u_1 and v_1 give lowest order (linear) equations (we shall go to higher order in these equations later):

$$(K_1^2 - 4\sigma u_{00}^2)u_1 + \Omega_1 u_{00} v_1 = 0, \tag{30}$$

$$\Omega_{10}u_1 + K_1^2 u_{00} v_1 = 0, \tag{31}$$

yielding linear dispersion relation

$$\Omega_{10}^2 = K_1^2(K_1^2 - 4\sigma u_{00}^2) \tag{32}$$

and lowest order connection

$$v_1 = -\frac{\rho}{u_{00}}u_1, \tag{33}$$

where $\rho=\Omega_{10}/K_1^2=\sqrt{1-4\sigma\zeta}$ and $\zeta=(u_{00}/K_1)^2$ are important parameters in the problem.

Next, we take variations with respect to u_2 and v_2. This, after use of Eq. (33), to $O(u_1^2)$, results in

$$\left(-\frac{\Omega_{00}}{2} + 2K_1^2 - 3\sigma u_{00}^2\right)u_2 + \Omega_{10}u_{00}v_2 = \frac{3\sigma}{2}u_{00}u_1^2, \tag{34}$$

$$\frac{\rho}{2}u_2 + u_{00}v_2 = \frac{3}{8}\frac{\rho}{u_{00}}u_1^2. \tag{35}$$

We solve these equations for u_2 and v_2:

$$u_2 = \left(2\sigma\zeta - \frac{1}{4}\right)\frac{u_1^2}{u_{00}}, \tag{36}$$

$$v_2 = \rho\left(\frac{1}{2} - \sigma\zeta\right)\frac{u_1^2}{u_{00}^2}. \tag{37}$$

Now, we take variations with respect to u_1 and v_1 again, but go to higher order in u_1 and include the driving terms [compare to Eqs. (30) and (31)]. This, after use of Eqs. (33), (36), and (37), yields

$$(K_1^2 - \Omega_0 - 6\sigma u_0^2)u_1 + \Omega_1 u_0 v_1 + N_1 = \varepsilon\cos\Phi, \tag{38}$$

$$\Omega_1 u_0 u_1 + K_1^2 u_0^2 v_1 + N_2 = -\varepsilon u_{00}\cos\Phi, \tag{39}$$

where $N_1=12u_1^3(\rho^2/32\zeta-\zeta)$ and $N_2=(3\Omega_{10}u_1^3/8u_{00})(1-\sigma\zeta)$. Then, we use Eq. (39) to eliminate v_1 in Eq. (38) and obtain higher order dispersion relation [compare to Eq. (32)]

$$\Omega_1^2 - K_1^2(K_1^2 + 2\Omega_0) + qu_1^2 = \frac{\varepsilon\Omega_{10}}{u_1}(1+\rho^{-1})\cos\Phi, \tag{40}$$

where $q=12(2u_{00}^2-\sigma K_1^2)$. Finally, we take variations with respect to Θ and ξ, to get two slow evolution equations

$$(\partial\Lambda/\partial\Omega_1)_t = \frac{\varepsilon}{2}s\sin\Phi \tag{41}$$

and

$$(\partial\Lambda/\partial\Omega_0)_t = \frac{\varepsilon}{2}s\sin\Phi. \tag{42}$$

These equations yield the conservation law

$$\partial\Lambda/\partial\Omega_0 - \partial\Lambda/\partial\Omega_1 \approx 2u_0u_1v_1 + 2u_0^2 + u_1^2 = \text{const}, \tag{43}$$

which, upon use of Eq. (33) and zero initial conditions on u_1 and v_1, gives

$$u_0^2 = u_{00}^2 + (\rho - 1/2)u_1^2. \tag{44}$$

Then, from Eq. (29),

$$\Omega_0 = -2\sigma[u_{00}^2 + (1+\rho)u_1^2]. \tag{45}$$

The last two equations can be used in Eq. (40) to rewrite it as

$$\Omega_1^2 - \Omega_{10}^2 + ru_1^2 = \frac{\varepsilon\Omega_{10}}{u_1}(1+\rho^{-1})\cos\Phi, \tag{46}$$

where $r=4K_1^2(6y-2\sigma+\sigma\rho)$. Finally, we use Eq. (46) to find the approximate expression for the frequency shift $\delta\Omega_1=\Omega_1-\Omega_{10}$ near the linear resonance:

$$\delta\Omega_1 \approx -2\left(6\frac{y}{\rho} - \frac{2\sigma}{\rho} + \sigma\right)u_1^2 + \frac{\varepsilon}{2u_1}(1+\rho^{-1})\cos\Phi. \tag{47}$$

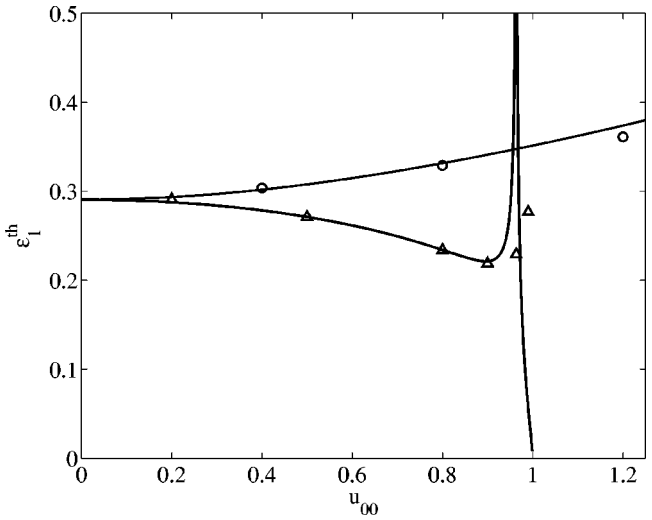

FIG. 6. The threshold ε_1^{th} for synchronization of 1-band NLS waves versus parameter u_{00}. Numerical thresholds for focusing ($\sigma=+1$, triangles) and defocusing ($\sigma=-1$, circles) 1-band NLS solutions are compared with analytical predictions, Eq. (50) (solid lines). Note that $u_{00}<1$ for stability in the focusing case in our example. The spike in the analytic result at $u_{00}=0.96$ ($\rho=0.27$) in this case corresponds to vanishing $O(u_1^2)$ frequency shift. Higher order nonlinear frequency corrections must be added in the theory to explain deviation from the simulation results in the vicinity of the spike.

C. Threshold for synchronization

At this stage, we use Eqs. (45) and (47) to write the evolution equation for the phase mismatch Φ. Assuming passage through linear resonance at $t=0$, i.e., $\omega_1=\Omega_{10}+\Omega_{00}-\alpha t$, we obtain

$$\Phi_t=\omega_1-\Omega_1-\Omega_0=-\alpha t+\sigma F(\rho)u_1^2-\frac{\widetilde{\varepsilon}}{2u_1}\cos\Phi, \quad (48)$$

where $F=4-\rho-\rho^{-1}$ and $\widetilde{\varepsilon}=\varepsilon(1+\rho^{-1})$. We supplement this equation by Eq. (41), which can be written as $(u_0u_1v_1)_t=\varepsilon(1+\rho)u_1\sin\Phi$ or, to lowest order,

$$u_{1t}=-(\widetilde{\varepsilon}/2)\sin\Phi. \quad (49)$$

Now, we focus on $F>0$ case (i.e., $0.27<\rho<3.73$), set $\alpha=\sigma|\alpha|$, define $A^2\equiv|\alpha|^{-1/2}Fu_1^2$, $\eta=\frac{1}{2}\widetilde{\varepsilon}F^{1/2}|\alpha|^{-3/4}$, and introduce new complex dependent variable $\Psi=A\exp(i\Phi)$. Then, Eqs. (48) and (49) reduce to Eq. (11) for Ψ. Consequently, we again encounter the characteristic threshold phenomenon (see Sec. III), i.e., η must exceed 0.411 for capture into resonance and subsequent synchronization. By returning to our original parameters, we find the threshold driving amplitude for synchronization:

$$\varepsilon_1^{th}=\frac{0.822|\alpha|^{3/4}\rho}{(1+\rho)|F|^{1/2}}, \quad (50)$$

where $|F|$ replaces F to include $F<0$ case. Figure 6 shows this threshold versus u_{00} (solid lines) and compares it with the results of numerical simulations (triangles for $\sigma=+1$ and circles for $\sigma=-1$) in the case $k_0=2$, and $\alpha=0.02$. Note that $u_{00}<1$ in our focusing NLS example ($\sigma=+1$) for stability. Generally, a very good agreement between the analytic prediction and simulations is observed except in the vicinity of the spike in the analytic result at $u_{00}=0.96$ ($\rho=0.27$) in the focusing NLS case. We notice that, at the location of the spike, coefficient F in the lowest order nonlinear frequency shift in Eq. (48) vanishes. Therefore, we conjecture that the difference between the simulation and analytic results in the vicinity of the spike can be explained by the necessity of adding higher order nonlinear frequency shifts in the theory. Nevertheless, because of algebraic complexity, inclusion of higher than second order nonlinear frequency corrections within our perturbation scheme remained outside the scope of the present work. Finally, we observe that, as for 0-band solutions, the amplitude of the autoresonant 1-band solution has small oscillating modulations seen in Fig. 1, having characteristic frequency [compare to Eq. (13)]

$$\nu\approx\sqrt{2\eta|\alpha|A}=\sqrt{\varepsilon(1+\rho^{-1})|F|u_1}. \quad (51)$$

D. Instability of doubly resonant 1-band solutions

Now, we discuss instability of 1-band solutions in the case when two resonant drives are present at a time, as observed in our simulations (see Fig. 1). We consider the driven system [compare to Eqs. (8) and (14)]

$$i\psi_t+\psi_{xx}+2\sigma|\psi|^2\psi=\varepsilon_0\exp(i\varphi_{d0})+\varepsilon_1\exp(i\varphi_{d1}), \quad (52)$$

where, as in Secs. III and IV A–IV C, $\varphi_{d0}=-\phi_0(t)$, $\varphi_{d1}=k_0x-\phi_1(t)$ and $d\phi_{0,1}/dt=\omega_{0,1}$, but both resonant drives are present at a time. We assume that autoresonant excitation of 0-band (spatially uniform) solution takes place first, reaching amplitude $|\psi|=u_0$ at some time t_1 as described in Sec. III. We shall also assume that at t_1 the system resonates with the second drive, so that one expects excitation of a 1-band solution beyond this time as described in Sec. IV A. However, in contrast to Sec. IV A, we do not switch off ε_0, so both drives resonate beyond t_1. Our goal is to investigate stability of this doubly resonant 1-band solution via the Whitham's approach.

We use representation (19), $\psi=U(\Theta,t)\exp[i(\xi+V(\Theta,t))]$, with definitions (21) and (22), covering both 0- and 1-band solutions in calculating the averaged Lagrangian Λ in the problem. Obviously, Λ has the same unperturbed part as in Eq. (23), but a more complicated driving term [compare to Eq. (28)]

$$\Lambda_d=\varepsilon_0u_0\cos\Phi_0+\frac{\varepsilon_1}{2}s\cos\Phi_1, \quad (53)$$

where $\Phi_0=\xi-\varphi_{d0}$, $\Phi_1=\Theta+\xi-\varphi_{d1}$, $s\approx u_1(1+\rho)$ and both phase mismatches $\Phi_{0,1}$, are assumed to be bounded and slow (synchronization assumption). The variational amplitude equations (41) and (42) of Sec. IV B in this case transform into

$$\left(\frac{1}{2}u_0u_1v_1\right)_t=\frac{\varepsilon_1}{2}u_1(1+\rho)\sin\Phi_1, \quad (54)$$

$$\left(\frac{1}{2}u_0^2+\frac{1}{4}u_1^2\right)_t=-\varepsilon_0 u_0\sin\Phi_0-\frac{\varepsilon_1}{2}(1+\rho)\sin\Phi_1 \quad (55)$$

or, by using lowest order relation (33) and combining the two equations,

$$u_{1t}=-\frac{\varepsilon_1}{2}(1+\rho^{-1})\sin\Phi_1, \quad (56)$$

$$u_{0t}=-\varepsilon_0\sin\Phi_0+\frac{\varepsilon_1 u_1}{4u_0}(\rho^{-1}-2\rho-1)\sin\Phi_1, \quad (57)$$

where, as before, $\rho=\Omega_{10}/K_0^2$. We also add variational equations (29) and (40), valid in the two drive case, i.e.,

$$\Omega_0=-\sigma(2u_0^2+3u_1^2), \quad (58)$$

$$\Omega_1^2-K_1^2(K_1^2+2\Omega_0)+12(2u_0^2-\sigma K_1^2)u_1^2=0, \quad (59)$$

where, assuming sufficiently large excitations ($\varepsilon\Omega_{10}/2u_1 \ll 1$), we neglect the driving term in Eq. (40). Next, we use Eq. (58) in Eq. (59) to write

$$\Omega_1^2-K_1^2(K_1^2-4\sigma u_0^2)+6(4u_0^2-\sigma K_1^2)u_1^2=0,$$

and seek solution for u_0 in the form $u_0=u_{00}+\delta u_0$, where u_{00} is the value at the linear resonance and $|\delta u_0|/u_{00}\ll 1$. Then, upon expansion in Eq. (58) and in the last equation,

$$\Omega_0\approx-\sigma(2u_{00}^2+4u_{00}\delta u_0+3u_1^2), \quad (60)$$

$$\Omega_1\approx\Omega_{10}-\frac{4\sigma u_{00}}{\rho}\delta u_0+3\sigma\rho u_1^2. \quad (61)$$

Finally, we use Eqs. (60) and (61) to write evolution system $\Phi_{0t}=\omega_0-\Omega_0$ and $\Phi_{1t}=\omega_1-\Omega_1-\Omega_0$ for the phase mismatches,

$$\Phi_{0t}=2\sigma u_{00}^2-\omega_0+4\sigma u_{00}\delta u_0+3\sigma u_1^2, \quad (62)$$

$$\Phi_{1t}=2\sigma u_{00}^2-\Omega_{10}-\omega_1+4\sigma u_{00}(1+\rho^{-1})\delta u_0+3\sigma(1-\rho)u_1^2. \quad (63)$$

Equations (54), (55), (62), and (63) comprise a complete set of coupled ordinary differential equations describing evolution of δu_0, u_1, and $\Phi_{0,1}$ in the two drive case. The analysis of this system of equations follows next.

We seek solutions of Eqs. (54), (55), (62), and (63) of the form $\delta u_0=\overline{\delta u_0}+\Delta u_0$, $u_1=\overline{u_1}+\Delta u_1$, $\Phi_{0,1}=\overline{\Phi}_{0,1}+\Delta\Phi_{0,1}$, where $\Delta u_{0,1}$ and $\Delta\Phi_{0,1}$ are small and oscillating, while $\overline{u}_{0,1}$ and $\overline{\Phi}_{0,1}$ are smooth, slowly evolving average components of the corresponding dependent variables. We shall assume that $\overline{\Phi}_{0,1}$ are near zero or π, for $\sigma=+1$ or -1, respectively. We shall also assume that the averaged components are determined by the slow quasiequilibrium of Eqs. (54), (55), (62), and (63):

$$\overline{u_{1t}}=-\frac{\varepsilon_1}{2}(1+\rho^{-1})\sin\overline{\Phi}_1,$$

$$\overline{u_{0t}}=-\varepsilon_0\sin\overline{\Phi}_0+\frac{\varepsilon_1\overline{u_1}}{4u_0}(\rho^{-1}-2\rho-1)\sin\overline{\Phi}_1,$$

$$2\sigma u_{00}^2-\omega_0+4\sigma u_{00}\overline{\delta u_0}+3\sigma\overline{u_1^2}=0,$$

$$2\sigma u_{00}^2-\Omega_{10}-\omega_1+4\sigma u_{00}(1+\rho^{-1})\overline{\delta u_0}+3\sigma(1-\rho)\overline{u_1^2}=0.$$

Then, by linearization in Eqs. (54), (55), (62), and (63), one obtains a system for $\Delta u_{1,2}$ and $\Delta\Phi_{0,1}$

$$\Delta u_{1t}=-\frac{\sigma\varepsilon_1}{2}(1+\rho^{-1})\Delta\Phi_1,$$

$$\Delta u_{0t}=-\sigma\left[\varepsilon_0\Delta\Phi_0+\frac{\varepsilon_1\overline{u_1}}{4u_0}(\rho^{-1}-2\rho-1)\Delta\Phi_1\right],$$

$$\Delta\Phi_{0t}=\sigma[4u_{00}\Delta u_0+6\overline{u_1}\Delta u_1],$$

$$\Delta\Phi_{1t}=\sigma[4u_{00}(1+\rho^{-1})\Delta u_0+6\sigma(1-\rho)\overline{u_1}\Delta u_1].$$

We seek solutions of this system in the form $\Delta u_{0,2}$, $\Delta\Phi_{1t}\sim\exp(-i\nu t)$. This yields the characteristic equation

$$(\nu^2-\nu_0^2)(\nu^2-\nu_1^2)-b=0, \quad (64)$$

where $\nu_0^2=4\varepsilon_0 u_{00}$, $\nu_1^2=\varepsilon_1\overline{u_1}(1+\rho^{-1})(4-\rho^{-1}-\rho)$, and $b=8\varepsilon_0\varepsilon_1 u_{00}\overline{u_1}(1+\rho^{-1})(\rho+\rho^{-1}+2)$. If one of the driving amplitudes $\varepsilon_{0,1}$ vanishes, the characteristic frequencies become $\nu=\nu_{0,1}$ in accordance with Eqs. (13) and (51). When both drives are present, the characteristic equation yields two solutions

$$\nu_\pm^2=\frac{1}{2}(\nu_0^2+\nu_1^2)\pm\sqrt{\frac{1}{4}(\nu_0^2+\nu_1^2)^2+c}, \quad (65)$$

where $c=12\varepsilon_0\varepsilon_1 u_{00}\overline{u_1}(1+\rho+\rho^{-1}+\rho^{-2})$. One of $\nu_\pm^2$ in Eq. (65) is always negative because of the positiveness of c. This means instability, i.e., dephasing and saturation of the driven solution, as observed in numerical simulations with two drives present in the second excitation stage in Fig. 1. This completes our analysis of autoresonant 1-band NLS waves.

V. CONCLUSIONS

(a) We have suggested a method of excitation and control of N-band solutions (N phase waves) of the nonlinear Schrödinger (NLS) equation in the framework of pattern formation by synchronization (PFS). The PFS idea, in general, is based on capturing the system into resonances with external driving perturbations having slowly varying frequencies and/or wave vectors. In the present application, we have considered spatially periodic NLS problem and successively perturbed the NLS equation by plane waves having different wave numbers $2\pi m/L$ (m being an integer and L the periodicity length) and slowly varying frequencies. Each frequency passed through a resonance in the system. The perturbing waves were arranged so that only a single drive was present at a time.

(b) The suggested excitation scheme started from zero and excited a spatially uniform (0-band) solution first, by passage through resonance with a small amplitude chirped frequency oscillation. The solution was continuously phase-locked (synchronized) with the drive despite the variation of the

driving frequency. The amplitude of the wave increased in the process of evolution to continuously match the nonlinear frequency shift of the driven solution to that of the driving oscillation. Such nonlinear, automatically synchronized evolution of a wave is usually referred to as wave autoresonance.

(c) We have switched off the uniform drive at some excitation stage of the 0-band solution and added a new traveling wave perturbation with a slowly chirped frequency. Passage through resonance with this perturbation yielded autoresonant excitation of a 1-band solution. Next, one could again switch off the drive and replace it by another plane wave with a different wave number and chirped frequency and so on. This process allowed autoresonant excitation of 2- and higher N-band solutions. Our approach was illustrated in numerical simulations, where the spectral analysis of the inverse scattering transform method for a periodic NLS system was used for diagnostics.

(d) We have studied excitation of spatially uniform (0-band) solutions by passage through resonance in more detail. This problem yields a universal single parameter ordinary differential equation (11) characteristic of many other resonantly driven wave applications (autoresonant excitation of 1-band solutions, for example). This equation describes the threshold phenomenon in autoresonant systems, i.e., the existence of a critical value of the driving amplitude above which the capture into resonance is guaranteed. This critical amplitude scales as $|\alpha|^{3/4}$, α being the driving frequency chirp rate.

(e) We have also studied autoresonant excitation of 1-band solutions via a weakly nonlinear version of the Whitham's averaged variational principle. This approach allows to reduce the fundamental equation (11) for this problem. The threshold amplitudes predicted by this theory were in a good agreement with simulations. It was also shown, by using the Whitham's approach, that simultaneous presence of two drives in the process of excitation of 0- and 1-band solutions results in instability, as observed in numerical simulations.

(f) Our analytic theory was limited to autoresonant 0- and 1-band solutions. Nevertheless, numerically, we have observed successive excitation of N-band waves with $N>1$ for both the focusing and defocusing NLS systems. The theory of such synchronized adiabatic excitations (possibly within the IST approach), particularly the theory of thresholds for capture into resonance, as well as applications to other systems exhibiting N-band solutions (sine-Gordon equation, for example) seem to comprise a set of interesting goals for future research in the field.

ACKNOWLEDGEMENTS

This work was supported by Israel Science Foundation (Grant No. 187/02), INTAS (Grant No. 03-51-4286), and RFBR (Grant N0. 03-02-16350).

APPENDIX A: FREQUENCIES OF 0- AND 1-BAND SOLUTIONS VIA IST APPROACH

The IST is a convenient method for describing N-band solutions of the periodic NLS equation. The details of this application of the method can be found elsewhere [4,5,19]. This appendix presents only minimal information from the IST theory, necessary for our analysis. It is known [19] that N-band NLS solutions can be constructed from a set of $2N+2$ parameters λ_k (the main spectrum) and a set of N variables $\mu_j(x,t)$ (auxiliary spectrum). The main spectrum is constant in time and, for the focusing NLS ($\sigma=+1$), consists of $N+1$ complex conjugate pairs, while in the defocusing case ($\sigma=-1$), all λ_k are real. The auxiliary spectrum components are functions depending on space and time via N phases $\Theta_n=K_n x-\Omega_n t$ of the N-band solution. In other words, $\mu_j=\mu_j(\Theta_1,\Theta_2,\ldots,\Theta_N)$ is a 2π-periodic function of its arguments. If all λ_k and μ_j and the value of ψ are given at initial time t_0 and position x_0, the corresponding N-band solution can be constructed by solving the following set of evolution equations in x and t [19]:

$$\mu_{jx}=\frac{-2i\sigma_j\left[\prod_{k=1}^{2N+2}(\mu_j-\lambda_k)\right]^{1/2}}{\prod_{l\neq j}(\mu_j-\mu_l)}, \tag{A1}$$

$$\mu_{jt}=\left(\sum_{k=1}^{2N+2}\lambda_j-2\sum_{m\neq j}\mu_m\right)\mu_{jx}, \tag{A2}$$

$$i\partial_t\ln\psi=\frac{3}{2}\left(\sum_{k=1}^{2N+2}\lambda_j\right)^2-2\sum_{j>k}\lambda_j\lambda_k-2\left(\sum_{k=1}^{2N+2}\lambda_k\right)\left(\sum_{k=1}^{N}\mu_k\right)+4\sum_{j>k}\mu_j\mu_k, \tag{A3}$$

$$i\partial_x\ln\psi=\sum_{k=1}^{2N+2}\lambda_j-2\sum_{j=1}^{N}\mu_j, \tag{A4}$$

where $\sigma_j=\pm1$ depending on which sheet of the Riemann surface defined by $[P(z)]^{1/2}=[\Pi_{k=1}^{2N+2}(z-\lambda_k)]^{1/2}$ the variable μ_j is on. Formally, the last two equations can be written as

$$i\partial_t\ln\psi=V_1(\boldsymbol{\Theta}),\quad i\partial_x\ln\psi=V_2(\boldsymbol{\Theta}), \tag{A5}$$

where $\boldsymbol{\Theta}=[\Theta_1,\Theta_2,\ldots,\Theta_N]$, while $V_{1,2}$ are 2π-periodic functions of all N arguments. Then, by writing $\psi=U\exp(i\Phi)$, $\mathrm{Im}(U,\Phi)=0$, we find evolution equations

$$\partial_t\ln U=\mathrm{Im}[V_1(\boldsymbol{\Theta})],\quad \partial_x\ln U=\mathrm{Im}[V_2(\boldsymbol{\Theta})],$$

and

$$\Phi_t=-\mathrm{Re}[V_1(\boldsymbol{\Theta})],\quad \Phi_x=-\mathrm{Re}[V_2(\boldsymbol{\Theta})].$$

Therefore, the general N-band solution can be written as

$$\psi(x,t)=U(\boldsymbol{\Theta})\exp\{i[\xi+V(\boldsymbol{\Theta})]\}, \tag{A6}$$

where both U and V are real periodic functions of all $\boldsymbol{\Theta}$ components, while the frequency and wave number associated with the external phase ξ are

$$\Omega_0\equiv-\xi_t=\langle\mathrm{Re}V_1(\boldsymbol{\Theta})\rangle_{\boldsymbol{\Theta}}, \tag{A7}$$

$$K_0\equiv\xi_x=-\langle\mathrm{Re}V_2(\boldsymbol{\Theta})\rangle_{\boldsymbol{\Theta}}, \tag{A8}$$

and $\langle\ldots\rangle_{\boldsymbol{\Theta}}$ means averaging over all Θ_k.

Now, we apply these results to cases $N=0,1(\sigma=+1)$. There exists only a single nondegenerate pair of main spectrum components, say $\lambda_1^{\pm}=a_1\pm ib_1$, for $N=0$ case. Then, from Eqs. (A3) and (A4), $V_1=4a_1^2-2b_1^2$, $V_2=2a_1$, and, therefore, $\psi=U_0\exp(i\xi)$, where $U_0=\text{const}$, while the external phase $\xi=K_0x-\Omega_0t+\xi_0$, $\xi_0=\text{const}$, where

$$\Omega_0=4a_1^2-2b_1^2,\quad K_0=-2a_1. \tag{A9}$$

In $N=1$ case, the solution has the form $\psi=U(\Theta_1)\exp i[\xi+V(\Theta_1)]$, and there are two pairs of nondegenerate, complex conjugate components $\lambda_{1,2}^{\pm}=a_{1,2}\pm ib_{1,2}$ in the main spectrum and the corresponding single auxiliary spectrum component μ_1. Then, from Eqs. (A3), (A4), (A7), and (A8) we find

$$\Omega_0=4(a_1^2+a_2^2+a_1a_2)-2(b_1^2+b_2^2)-4(a_1+a_2)\langle\mathrm{Re}\mu_1\rangle, \tag{A10}$$

$$K_0=-2(a_1+a_2)+2\langle\mathrm{Re}\mu_1\rangle. \tag{A11}$$

At the same time, Eq. (A2) yields the phase velocity associated with the internal phase

$$\Omega_1/K_1=\sum\lambda_j=2(a_1+a_2). \tag{A12}$$

Thus, if wave numbers K_0 and K_1 of the 1-band solution are known, Eqs. (A10)–(A12) yield the associated frequencies Ω_0 and Ω_1 via the relevant nondegenerate pairs of the main spectrum.

APPENDIX B: WEAKLY NONLINEAR AVERAGED VARIATIONAL PRINCIPLE

We describe our driven NLS system via variational principle (17)

$$\delta\left(\int\int dxdtL(U,U_x,U_t,\theta_x,\theta_t,t)\right)=0, \tag{B1}$$

where Lagrangian $L=L_0+L_1$, its unperturbed part is

$$L_0=\frac{1}{2}[U_x^2+U^2(\theta_x^2+\theta_t)]-\frac{\sigma}{2}U^4, \tag{B2}$$

and $L_1=\varepsilon U\cos(k_0x-\phi_1-\theta)$ represents the driving perturbation. The Whitham's approach [20] to the problem is a perturbation expansion based on representing solutions of our driven system as slowly modulated solutions of the unperturbed system. To this end we write [12] $U=U(\Theta,t)$ and $\theta=\xi+V(\Theta,t)$, where $\Theta=K_1x-\int\Omega_1(t)dt$, $K_1=mk_0$, $\xi=K_0x-\int\Omega_0(t)dt$, and the explicit time dependence in $V(\Theta,t)$ and $\Omega_{0,1}(t)$ is due to the perturbation, and assumed to be slow. The unperturbed Lagrangian L_0 in this representation becomes a function of a *single* independent fast angle variable Θ and assumes the form $L_0(U,U_\Theta,V_\Theta)=1/2\{K_1^2U_\Theta^2+U^2[(K_0+K_1V_\Theta)^2-(\Omega_0+\Omega_1V_\Theta)]\}-(\sigma/2)U^4$. This Lagrangian describes a two-degrees-of-freedom (U,V) dynamical problem in Θ, where V is a cyclic variable. The problem possesses two constants of motion $E=U_\Theta(L_0)_U+V_\Theta(L_0)_V-L_0$ ("energy") and $M=(L_0)_{V_\Theta}=[2K_1(K_0+K_1V_\Theta)-\Omega_1]U^2$ ("momentum") and, therefore, is integrable. Now, one can express V_Θ in terms of U and M

$$V_\Theta=\frac{\Omega_1}{2K_1^2}-\frac{K_0}{K_1}+\frac{M}{2K_1^2U^2}, \tag{B3}$$

which, upon substitution into the expression for E yields a one-degree-of-freedom problem for U, which can be integrated in quadratures. This problem describes oscillations of U in a one-dimensional quasipotential and we view Θ as a canonical angle variable of these oscillations. Then, U [and V via Eq. (B3)] in the unperturbed problem becomes a 2π-periodic function of Θ. In the presence of forcing in our application, E,M, as well as, $\Omega_{0,1}$ become slow functions of time. The evolution of these slow variables is described by Whitham's averaged variational principle,

$$\delta\left(\int\int dxdt\Lambda(E,M,K_0,\Omega_0,K_1,\Omega_1,\Phi)\right)=0, \tag{B4}$$

where the averaged Lagrangian Λ is obtained by averaging $L=L_0+L_1$ over one period, 2π, of the fast angle variable Θ, keeping the slow time dependence in $L_{0,1}$ fixed. The object Φ in the averaged Lagrangian is the phase mismatch ($\Phi=\Theta+\xi-\varphi_{d1}$ in the case of interest), assumed to be slow in the phase-locked solution. Variations in Eq. (B4) with respect to E, M, Θ, and ξ yield the desired slow evolution equations in our driven problem. This is the essence of the fully nonlinear Whitham's approach [12] to excitation of synchronized 1-band NLS waves. Since the problem of thresholds in the present application is a weakly nonlinear phenomenon, we shall use a weakly nonlinear version of the Whitham's method.

In the weakly nonlinear case we write [see Eq. (21)]

$$U\approx u_0+u_1\cos\Theta+u_2\cos2\Theta, \tag{B5}$$

where u_i are slow amplitudes ordered as $u_0\sim O(1)$; $|u_1|\ll1$, and $u_2\sim O(u_1^2)$. Then, from Eq. (B3), the weakly nonlinear form of V is

$$V\approx-v_1\sin\Theta-v_2\sin2\Theta, \tag{B6}$$

where the slow amplitudes are ordered as $v_1\sim O(u_1)$, $v_2\sim O(u_1^2)$, while $\langle V\rangle_\Theta=0$ since the averaged part of $\theta=\xi+V$ can always be included in ξ. Substitution of Eqs. (B5) and (B6) into L and averaging over Θ yields the following averaged Lagrangian [to $O(u_1^4)$]:

$$\Lambda=-\frac{\sigma}{2}\Lambda_0-\frac{\Omega_0}{4}\Lambda_1+\frac{\Omega_1}{4}\Lambda_2+\frac{K_1^2}{4}\Lambda_3+\Lambda_d, \tag{B7}$$

where

$$\Lambda_0 = u_0^4 + 3u_0u_1^2u_2 + 3u_0^2(u_1^2 + u_2^2) + 3u_1^4/8, \tag{B8}$$

$$\Lambda_1 = 2u_0^2 + u_1^2 + u_2^2, \tag{B9}$$

$$\Lambda_2 = 2u_0u_1v_1 + u_1v_1u_2 + u_1^2v_2 + 4u_0u_2v_2, \tag{B10}$$

$$\Lambda_3 = u_1^2 + 4u_2^2 + v_1^2(u_0^2 + 3u_1^2/4 + u_0u_2) + 4u_0u_1v_1v_2 + 4u_0^2v_2^2, \tag{B11}$$

and only the term with the relevant (slow) phase mismatch, $\Phi = \Theta + \xi - \varphi_{d1}$, is left in the driving part of the Lagrangian after the averaging,

$$\Lambda_d = \frac{\varepsilon}{2}(u_1 - u_0v_1)\cos\Phi. \tag{B12}$$

[1] M. J. Ablowitz and H. Segur, *Solitons and the Inverse Scattering Transform* (SIAM, Philadelphia, 1981).
[2] S. C. Gardner, J. M. Greene, M. D. Kruskal, and R. M. Miura, Phys. Rev. Lett. **19**, 1095 (1967).
[3] V. E. Zakharov and A. B. Shabat, Sov. Phys. JETP **34**, 62 (1972).
[4] Y. Ma and M. J. Ablowitz, Stud. Appl. Math. **65**, 113 (1981).
[5] E. R. Tracy and H. H. Chen, Phys. Rev. A **37**, 815 (1988).
[6] M. Deutsch, B. Meerson, and J. Golub, Phys. Fluids B **3**, 1773 (1991).
[7] I. Aranson, B. Meerson, and T. Tajima, Phys. Rev. A **45**, 7500 (1992).
[8] L. Friedland, Phys. Fluids B **4**, 3199 (1992).
[9] L. Friedland, Phys. Rev. Lett. **69**, 1749 (1992).
[10] L. Friedland, Phys. Rev. E **55**, 1929 (1997).
[11] L. Friedland, Phys. Rev. E **57**, 3494 (1998).
[12] L. Friedland, Phys. Rev. E **58**, 3865 (1998).
[13] L. Friedland and A. G. Shagalov, Phys. Rev. Lett. **81**, 4357 (1998).
[14] L. Friedland, Phys. Rev. E **59**, 4106 (1999).
[15] L. Friedland and A. G. Shagalov, Phys. Rev. Lett. **85**, 2941 (2000).
[16] L. Friedland and A. G. Shagalov, Phys. Fluids **14**, 3074 (2002).
[17] L. Friedland and A. G. Shagalov, Phys. Rev. Lett. **90**, 074101 (2003).
[18] M. Khasin and L. Friedland, Phys. Rev. E **68**, 066214 (2003).
[19] E. R. Tracy, H. H. Chen, and Y. C. Lee, Phys. Rev. Lett. **53**, 218 (1984).
[20] G. B. Whitham, *Linear and Nonlinear Waves* (Wiley, New York, 1974).
[21] C. Canuto, M. Y. Hussaini, A. Quarteroni, and T. A. Zang, *Spectral Methods in Fluid Dynamics* (Springer-Verlag, New York, 1988).
[22] S. Ahmad and A. R. Chawdhury, J. Math. Phys. **28**, 134 (1987).
[23] J. Fajans, E. Gilson, and L. Friedland, Phys. Rev. Lett. **82**, 4444 (1999).
[24] L. Friedland, Astrophys. J. Lett. **547**, L75 (2001).
[25] E. Grosfeld and L. Friedland, Phys. Rev. E **65**, 046230 (2002).
[26] G. Marcus, L. Friedland, and A. Zigler, Phys. Rev. A **69**, 013407 (2004).
[27] L. Friedland, Phys. Plasmas **5**, 645 (1998).